International Journal of Pharmaceutics 650 (2024) 123697

Contents lists available at ScienceDirect

International Journal of Pharmaceutics

journal homepage: www.elsevier.com/locate/ijpharm

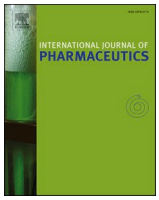

# Microfluidic development and biological evaluation of targeted therapy-loaded biomimetic nano system to improve the metastatic melanoma treatment

Ilaria Arduino [a], Roberta Di Fonte [b], Mattia Tiboni [c], Letizia Porcelli [b], Simona Serrati [b], Dafina Fondaj [a], Tania Rafaschieri [b], Annalisa Cutrignelli [a], Gabriella Guida [d], Luca Casettari [c], Amalia Azzariti [b,*], Angela Assunta Lopedota [a], Nunzio Denora [a], Rosa Maria Iacobazzi [a,*]

[a] Department of Pharmacy–Pharmaceutical Sciences, University of Bari, 70125 Bari, Italy
[b] IRCCS Istituto Tumori "Giovanni Paolo II", 70124 Bari, Italy
[c] Department of Biomolecular Sciences, University of Urbino Carlo Bo, Piazza del Rinascimento 6, 61029 Urbino, Italy
[d] Department of Traslational Biomedicine and Neuroscience (DiBraiN), School of Medicine, University of Bari "A. Moro", 70124 Bari, Italy

ARTICLE INFO

*Keywords:*
Microfluidics
Biomimetic
Hybrid liposomes
Cell membrane
Cancer therapy

ABSTRACT

Optimizing current therapies is among next steps in metastatic melanoma (MM) treatment landscape. The innovation of this study is the design of production process by microfluidics of cell membrane (CM)-modified nanoparticles (NPs), as an emerging biomimetic platform that allows for reduced immune clearance, long blood circulation time and improved specific tumor targeting. To achieve melanoma selectivity, direct membrane fusion between synthetic liposomes and CMs extracted from MM cell line was performed by microfluidic sonication approach, then the hybrid liposomes were loaded with cobimetinib (Cob) or lenvatinib (Lenva) targeting agents and challenged against MM cell lines and liver cancer cell line to evaluate homotypic targeting and antitumor efficacy. Characterization studies demonstrated the effective fusion of CM with liposome and the high encapsulation efficiency of both drugs, showing the proficiency of microfluidic-based production. By studying the targeting of melanoma cells by hybrid liposomes versus liposomes, we found that both NPs entered cells through endocytosis, whereas the former showed higher selectivity for MM cells from which CM was extracted, with 8-fold higher cellular uptake than liposomes. Hybrid liposome formulation of Cob and Lenva reduced melanoma cells viability to a greater extent than liposomes and free drug and, notably, showed negligible toxicity as demonstrated by bona fide haemolysis test. The CM-modified NPs presented here have the potential to broaden the choice of therapeutic options in MM treatment.

## 1. Introduction

Nanoparticle (NP) based drug delivery technology (i.e., nanomedicine) has demonstrated the potential to improve clinical cancer therapy. The main advantages of NPs administration are reducing side effects by targeting specific cells, protecting critical drugs from premature degradation, improving the solubility of difficult-to-administer drugs, and their sustained and controlled release (Iacobazzi et al., 2022; Ricci et al., 2022; Sommonte et al., 2022). However, conventional NPs still face various biological bottlenecks, limiting their therapeutical potential (Zinger, 2023). Firstly, as exogenous materials, NPs after systemic administration are bound by proteins becoming more recognizable by phagocytic cells, and subsequently, they are rapidly cleared by the reticuloendothelial (RES) and mononuclear phagocytic systems (MPS), limiting their delivery and distribution (Chen et al., 2016). Thus, to efficiently enter lesion sites, NPs need to evade clearance by the immune system. The incorporation of polyethylene glycol (PEG) on the surface of NPs has been the most popular standard in the process to make them stealth, with less interaction with the surrounding environment, increasing their blood circulation time (Fondaj et al., 2023). However, immunological reactions due to the presence of anti-PEG antibodies following repeated administration have been reported, which could compromise the performance of such NPs. In light of this, the PEG dilemma has been questioned (Ishihara et al., 2009; Wu et al.,

* Corresponding authors.
*E-mail addresses:* a.azzariti@oncologico.bari.it (A. Azzariti), rosa.iacobazzi@uniba.it (R.M. Iacobazzi).

https://doi.org/10.1016/j.ijpharm.2023.123697
Received 1 September 2023; Received in revised form 6 December 2023; Accepted 8 December 2023
Available online 9 December 2023

2022; Yang and Lai, 2015; Zinger, 2023). Secondly, to achieve targeted drug delivery via NPs, several barriers must be overcome, and yet in most cases, the ability of a drug to have a therapeutic effect at its site of action is governed by the NPs' ability to enter the cell (Rennick et al., 2021). Thus, to achieve this goal, NPs mediated active targeting has been explored through surface-conjugation of specific target ligands such as antibodies, peptides, aptamers, or other small molecules. Recently, the employment of cellular membrane (CM) material for biomimetic NP formulation has emerged as a promising approach to get beyond these limitations as it has become evident that cells in our bodies have inherent the capacity to overcome these obstacles, mostly because of the characteristics of their cell membranes. Biomimetic NPs offer a flexible platform that could successfully address the challenges currently facing NPs by combining the advantages of natural cell membrane components with the production techniques and controllability of synthetic NP systems (Fang et al., 2014; Rampado et al., 2022; Zinger, 2023). This endeavour was motivated by the observation of natural as they have developed extremely specialized functionalities through time, which are challenging to completely replicate using synthetic materials (Oldenborg et al., 2000; Rodriguez et al., 2013; Tiboni et al., 2021a). Particularly, cancer cells, unlike most other membrane donors, are simple to cultivate in enormous quantities *in vitro*; they also have unique capacity to self-target homologous cells. Therefore, it is predicted that cancer CMs-coated or fused NPs will achieve homologous targeting, which is particularly ideal for targeting drug administration and efficient cancer therapy (Fondaj et al., 2023; Sun et al., 2016).

In this study, the focus is on hybrid biomimetic fused NPs, which involves the direct integration of CMs with the synthetic material of NPs (Fondaj et al., 2023). The biological components become part of the NPs structure physically or chemically by fusing with the main components of the NPs. This integration provides unique biological properties and functionality, such as specific targeting, enzymatic activity, or cell recognition (Fondaj et al., 2023) as well as greater uniformity of the chemical–physical and morphological characteristics of the nano system, resulting in better formulation stability. In particular, liposomes have been used as a biological membrane model to study the biological functions of living cells (Song et al., 2021). Obviously, liposomes lack complex antigens present on natural cell membranes. Specifically, here, we hypothesized that liposomes hybridized with CMs extracted from metastatic melanoma cell line, could combine the homologous targeted capacity of the natural CMs and the design versatility of the synthetic liposome, thus improving the delivery and therapeutic potential of drugs used to treat melanoma.

It is crucial for the development of a drug delivery system applicable in clinical cancer therapy is to optimize methods to guarantee that final products are standardized, batch-to-batch consistent, scalable, conform to good manufacturing practice (GMP), and adaptable to high-throughput assembly methods. To address these needs, microfluidics has emerged as a promising technique (Arduino et al., 2020; Iacobazzi et al., 2021; Molinaro et al., 2018). The conventional fabrication of biomimetic hybrid NPs involves the employment of mechanical extrusion through nanoporous membranes and ultrasonic energy, the destructive forces induced by sonication and extrusion could break the CMs and reassemble them by fusing with the lipids/polymers of the NPs (Chen et al., 2022; He et al., 2019; Himbert et al., 2022; Liu et al., 2018). These methods are labour-intensive and time-consuming and may suffer from large batch-to-batch differences in NPs properties. For these reasons, microfluidic platforms, capable of incorporating various reaction compartments, have emerged as possible tools for the controlled assembly of NPs. When compared to traditional methods, microfluidic techniques have proven to be undoubtedly quite effective in the production of biomimetic nanoparticles. Microfluidic methods are known for their gentle treatment of sensitive biomolecules, minimizing shear and thermal stress that could compromise their integrity. It allows researchers to fine-tune parameters such as flow rates and mixing ratios, resulting in nanoparticles that are not only consistent but also exceptionally well-defined in terms of size, shape, and composition. Microfluidic technique produces highly uniform nanoparticles with narrow size distributions, which improves reproducibility. Furthermore, these systems frequently achieve high encapsulation efficiency for bioactive molecules and drugs, lowering the risk of payload loss during manufacturing (Abreu et al., 2022; Fondaj et al., 2023). However, the challenge of disrupting CMs with purely hydrodynamic forces in microchannels limits the applicability of microfluidics to produce hybrid biomimetic systems. To solve this problem, in this study, we suggest coupling external force fields to microfluidic channels. Specifically, we propose the coupling of two strategies to promote mixing: active and passive mixing. Passive mixing is induced by the geometry of the employed microfluidic devices customized by 3D printing, while active mixing is caused by an external physical field, in this case, prompted by an ultrasonic bath.

Finally, to test whether the CM-modified hybrid liposomes produced in microfluidics had the potential to broaden the choice of therapeutic options in MM treatment, we encapsulated in such hybrid biomimetic liposomes two different anti-melanoma drugs: the MEK inhibitor cobimetinib (Cob), which is used to inhibiting the costitutive activation of MAPK occuring in metastatic melanoma harboring the BRAFV600 mutations (Porcelli et al., 2022), and the anti-angiogenic tyrosine kinase inhibitor lenvatinib (Lenva), which is currently under investigation in phase II clinical trials in combination with immunotherapy for the treatment of advanced melanoma (Stoff et al., 2023). Both the drugs' formulations were challenged against either BRAF wild type and BRAFV600 MM cell lines for assessing anti-tumour potential.

## 2. Materials and methods

### 2.1. Materials

All chemicals were purchased at the highest available purity and used as received without further purification or distillation. Polypropylene (PP) filament was purchased from BASF (Germany). L-α-Phosphatidylcholine from soybean, ≥ 99 % (TLC), lyophilized powder, Cholesterol, DPBS (Dulbecco's Phosphate Buffered Saline), Tween 80, PKH67 Fluorescent Cell Linker Kits (green, fluorescent dye), PKH26 Red Fluorescent, Dulbecco's Modified Eagle's medium (DMEM), heat-inactivated fetal bovine serum (FBS), human serum, Ethanol 99 % (v/v) (EtOH) and Dimethylsulfoxide (DMSO) were purchased from Sigma Aldrich. 1,2-dipalmitoyl-*sn*-glycero-3-phosphoethanolamine-N-(7-nitro-2–1,3-benzoxadiazol-4-yl) (ammonium salt) (NBD-PE) and 1,2-dipalmitoyl-*sn*-glycero-3-phosphoethanolamine-N- (lissamine rhodamine B sulfonyl) (Liss Rhod PE), were bought from Avanti Polar Lipids. Cobimetinib (Cob) and lenvatinib (Lenva) were purchased from Selleckchem.com.

### 2.2. Cell membrane isolation from BRAF wild-type human metastatic melanoma cell line

The cell membranes (CMs) were derived, from the BRAF wild type metastatic melanoma cell line, named MGS, in accordance to described protocols (Hu et al., 2015; Serratì et al., 2023). To isolate CMs, the pellet consisting of MGS cells was first lysed by the addition of MilliQ and then subjected to two cycles of freezing and thawing, to allow the breakdown of the cellular structure. Then the sample was sonicated, using an ultrasound probe tip (9 W) for two minutes at 4 °C and centrifuged at 15,000 RCF for 15 min at 4 °C three times. Finally, the sample was ultracentrifuged at 100,000 RCF for 60 min at 4 °C. The CMs were then redispersed in 0.2 mL water for injectable preparations and stored at −20 °C. To analyse the protein content of CMs the Bradford method was conducted (Sommonte et al., 2023a).

### 2.3. Fabrication of microfluidic device by 3D printing

The microfluidic devices were developed and produced as reported before (Khorshid et al., 2022). Briefly, the chip designs were produced using a CAD software while the relative STereo Lithography interface formats (STL) were printed using a polypropylene filament in a fused deposition modeling (FDM) 3D printer (Ultimaker 3, Ultimaker, The Netherlands). The printing parameters were maintained for both devices with a print speed of 25 mm/s at a temperature of 220 °C through a 0.25 mm nozzle. The infill density was 100 %, and the built plate was kept at 85 °C and covered with a polypropylene adhesion sheet (Ultimaker, The Netherland). Alternating 50 μm thick layers were printed with a perpendicular pattern compared to the length of the device, enabling leak-free and semi-transparent devices to be printed with PP. Stainless steel probe needles were used to connect the chip to pump tubing. To confirm the effective printing of the channels, a colored aqueous solution was pumped into each microchannel to evaluate the flow patterns.

### 2.4. Preparation of fused hybrid liposomes by microfluidic technique

The hybrid liposomes were prepared using two different 3D-printed microfluidics devices, comparing co-flow with a T-shape geometry. The organic phase consisted of a mixture of 4.2 mg/mL of phosphatidylcholine from soybean and 0.8 mg/mL of cholesterol in ethanol and 1 mg/mL of Cob or Lenva. The aqueous phase consisted of just PBS for liposomes while PBS and CMs (equal to 0.2, 0.4, or 0.6 mg of CM protein contents) for hybrid liposomes. The organic and aqueous phases corresponded to the inner and outer phases, respectively. With the usage of two microfluidics pumps, we set the flow rate of the inner (1 mL/min) and the outer solution (3 mL/min) and we kept the flow-rate constant. The liquids flowed from their respective syringes into the devices through tiny tubes. During the preparation of all formulations, the microfluidic devices were subjected to sonication using a bath sonicator (CP102 Ultrasonic Cleaner, France) at a frequency of 60 kHz and a power of 400 W. The resulting preparations were subsequently purified by ultracentrifugation at 45000 rpm at 4 °C for 120 min. To determine the cellular uptake of liposomes and hybrid liposomes, the formulation contained a fluorescent lipid. In particular, 17 μg of Liss Rhod PE was added to the organic phase.

### 2.5. Membrane-lipids fusion validation by FRET and flow cytometry colocalization study

To conduct the Förster resonance energy transfer (FRET) study, two fluorescent lipids were employed during biomimetic NPs production: 1,2-dipalmitoyl-*sn*-glycero-3-phosphoethanolamine-N-(7-nitro-2–1,3-benzoxadiazol-4-yl) (ammonium salt) (NBD-PE, excitation/emission = 463/536 nm) and 1,2-dipalmitoyl-*sn*-glycero-3-phosphoethanolamine-N-(lissamine rhodamine B sulfonyl) (Liss Rhod PE, excitation/emission = 560/580 nm). Both fluorescent lipids were dissolved in ethanol (inner phase). Briefly, fluorescent liposomes and hybrid liposomes were prepared by the same method, except that 1.7 μg of NBD-PE and 17 μg of Liss Rhod PE were dissolved in a lipid phase. The fluorescence spectrum of each sample was then read between 500 and 650 nm using an excitation wavelength of 470 nm on a Tecan Infinite M200 plate reader. Fluorescence recovery of the donor (NBD-PE) at the lower emission peak (534 nm) was used to indicate increasing amounts of fusion.

FRET efficiency, defined as the proportion of donor molecules (NBD) that have transferred their excess energy to the acceptor molecules (rhodamine), was calculated using the following equation as previously described (He et al., 2019; Song et al., 2021):

$$FRETEFFICIENCY(\%) = \frac{Fa}{(Fa + Fd)} \times 100$$

where Fa = emission fluorescence of acceptor (rhodamine) and Fd = emission fluorescence of donor (NBD).

The membrane colocalization study was conducted as previously described (He et al., 2019). CMs were labelled with PKH26 (excitation/emission = 551/567 nm), and lipid membranes were labelled with PKH67 (excitation/emission = 490/504 nm). The hybrid liposomes were prepared as described above using these dye-labelled membranes and were then analysed by FCM. Non labelled CMs and liposomes were used as the controls.

### 2.6. Particle size, size distribution, surface electrostatic charge and nanoparticle tracking analysis

The size distribution and ζ-potential of all preparations were evaluated using a Zetasizer Nano ZS (Malvern Instruments Ltd., Worcestershire, UK). Approximately 1 mL of a 1:50 diluted solution in double-distilled water of each sample was analysed using disposable polystyrene cuvettes (Sarstedt AG & Co., Germany) at 25 ± 0.1 °C (Racaniello et al., 2022). The surface ζ-potential was evaluated using 750 μL of the 1:50 dilution in demineralized water of the NPs suspension in a disposable folder capillary cell (DTS1070, Malvern, UK). The particle size distribution and concentration in solution as NPs/mL of the liposome and hybrid liposomes were analysed with the NanoSight NS300 (Malvern Panalytical) following the manufacturer's instructions (Serratì et al., 2022). All the experiments were performed in triplicate and the resulting data are shown as the numerical mean and standard deviation of each triplicate.

### 2.7. Evaluation of encapsulation efficacy (EE %)

The assessment of EE (%) of the formulation was conducted via the direct measurement of encapsulated Cob and Lenva. Briefly, 100 μL of drug-loaded liposome or hybrid liposome were lyophilized and destroyed using 500 μL of DMSO. The amount of drug was evaluated via spectroscopy. The absorbance measurements at λ = 320 nm for Cob and λ = 340 nm for Lenva, were carried out in triplicate at room temperature, by using a Tecan Infinite® 200 PRO plate reader (Tecan, Switzerland).

The EE % was calculated using Eq. (1).

$$\text{EE}\,(\%) = \frac{\text{mass of drug found into NPs}}{\text{mass of drug initially added}} \times 100 \quad (1)$$

### 2.8. Transmission electron microscopy (TEM) imaging

The NPs size, shape, and morphology were investigated according to a known procedure (Serratì et al., 2022). Briefly, a drop of NPs suspension was deposited onto a lacey carbon-coated copper TEM grid, 300 mesh. Then, the grid was stained with 1 % osmium tetroxide for 1 min prior to being rinsed with ultrapure water and let to dry. Low-magnification images were recorded on a JEOL Jem1011 microscope (Tokyo, Japan) operating at an accelerating voltage of 100 kV.

### 2.9. Drugs release profiles analysis

Studies of Cob and Lenva release from liposome and hybrid liposomes were conducted using Franz cells (Iacobazzi et al., 2021; Mantuano et al., 2021; Sommonte et al., 2023a). In brief, 500 μL of each formulation was placed on the diffusion barrier (area of 0.6 $cm^2$) constituted by an artificial cellulose acetate membrane (3.5 kDa, Fisher Scientific Milano), which divides donor and receptor cells. Phosphate buffer (PBS, pH 7.4) with 1 % (w/v) of Tween 80 was selected as the receptor medium and it was frequently stirred and retained at a temperature of (37 ± 0.5 °C). In an overall time of 72 h, 0.2 mL was picked up from the receiving compartment at set times, and to provide the sink conditions the equivalent volume of refreshed PBS was included in the receptor cell. The collected fractions were analysed by UV–Vis to

determine the drug content. Each experiment was performed in triplicate and was conducted in three separate Franz cells using three distinct batches of each formulation.

### 2.10. In vitro biological studies

#### 2.10.1. Cell culture

Human metastatic melanoma cell line MGS with BRAF wild type and Hmel-1 cell line with BRAF V600 mutation, were isolated from a tumour surgical specimen as described in (Zanna et al., 2013) and in Serratì S. and Di Fonte R., et al. (data submitted). Briefly, the tissue was washed twice in PBS and minced into small fragments with surgical blades under aseptic conditions and layered in a 60 mm dish with high-glucose Dulbecco's modified Eagle's medium (DMEM) supplemented with 10 % (v/v) fetal bovine serum (FBS), 1 % (v/v) l-glutamine, 1 % (v/v) penicillin/streptomycin, at 37 °C in a humidified atmosphere of 5 % $CO_2$. The cells growth around the fragments were harvested and cultured in complete DMEM. Human SK-HEP-1 cell line isolated from the liver of a male with adenocarcinoma, were purchased from American Type Culture Collection (ATCC, VA, USA). Cells were cultured in DMEM as previously reported (Iacobazzi et al., 2017).

For MGS spheroids formation, cells were seeded at a density of 5000 cells/well on 96 well plate Corning®Spheroid Microplate and incubated at 37 °C under 5 % $CO_2$ for 5 days before performing experiments. Spheroid formation was assessed using the Celldiscoverer 7 Live Cell Imaging System (Zeiss, Jena, Germany).

#### 2.10.2. Homotypic targeting studies on 2D and 3D cell models

The internalization studies were conducted *in vitro* both in 2D and 3D cell models by means of flow cytometry analysis (FCM) and fluorescence imaging (FI) according to a protocol described in (Arduino et al., 2021). The uptake studies in 2D have been conducted in the melanoma cells, from which we extracted the cell membranes, in Hmel-1 and SK-HEP-1 cell lines, incubating cells for 2 h with liposomes or hybrid liposome (0.5 μM in terms of Liss Rhod PE). The experiments were conducted at both 37 °C and 4 °C to evaluate the total fluorescence and the fluorescence associated exclusively with the cellular membrane. The flow cytometer used was AttuneNxT acoustic focusing cytometer (Thermo Fisher Scientific, Waltham, MA, USA). 10,000 events were counted in the viable gate and the geometric mean of the viable cell population exposed to NPS was used to determine their internalization, after correction for cell auto-fluorescence and for NPS compounds-autofluorescence. The data shown in the graphs are representative of the actual internalized fluorescence, calculated as the difference between the values obtained from the analysis at 37 °C and those obtained from the analysis at 4 °C. Data were interpreted using the Attune NxT Analysis Software (Thermo Fisher Scientific, Waltham, MA, USA) and the CytExpert software v.1.2, provided by the manufacturer and represent mean ± SD, n = 3.

The analysis of MGS 3D model was conducted by incubating spheroids for 2 h with rhodamine-hybrid liposomes and rhodamine-liposomes and for 30 min with Hoechst 33,342 dye (2 μg/mL, Invitrogen™) for nuclei staining. For the visualization on the Celldiscoverer 7 Cell Imaging System (Zeiss, Jena, Germany) with a Plan-Apochromat 20×/0.95 objective and optavar 0.5x tubelens, spheroids were washed and recovered with PBS without $Ca^{2+}$ and $Mg^{2+}$. The co-localization signal of the two fluorophores was quantified by circumscribing the internal area of the spheroid and by using the Zen 3.2 software for fluorescence intensity quantification (Carl Zeiss Microscopy, Germany).

#### 2.10.3. Endocytosis pathway inhibition

To study the endocytosis mechanism according to (Denora et al., 2013; Rennick et al., 2021) for hybrid liposomes and liposomes, MGS cells were pre-incubated with the following inhibitors for 2 h at 37 °C:

- LY294002 (50 nM), as an inhibitor of macropinocytosis,
- Potassium depletion buffer (K + DB, isotonic), as an inhibitor of the clathrin-mediated endocytosis, (composition: NaCl 140 mmol/L, HEPES 20 mmol/L, $CaCl_2$ 1 mmol/L, $MgCl_2$1 mmol/L, D-glucose 1 mg/mL, pH 7.4),
- Methyl-β-cyclodextrin (10 mM), as an inhibitor of the Clathrin-independent endocytosis

After that, the medium was removed, and the freshly prepared test compounds (Rhodamine-labelled hybrid liposomes and liposomes, 1 μM) in media containing inhibitors at the same concentrations were added and further incubated for 4 h. The cells after being washed three times with HBSS, were collected according to the methods described above and analysed via FCM to assess the uptake of the NPs. In this experiment, the group without any treatment was used as a background in the FCM, while the group in the presence of hybrid liposomes or liposomes but without inhibitor treatment was used as a control. The endocytosis inhibition was quantified by normalizing the geometric mean fluorescence of wells treated with an inhibitor to that of control wells. Alternatively, the cells were placed at 4 °C to investigate the effect of temperature on the internalization of NPS.

#### 2.10.4. Haemolysis test

In-vitro haemolysis of liposomes and hybrid liposomes was assessed using human whole blood kindly donated by a healthy volunteer person. Human whole blood was freshly diluted before the test as follows: 0.556 mL of human whole blood was added to 1.944 mL of sterile Dulbecco's PBS pH 7.4 and shaken gently. 1 mL of this suspension was withdrawn and added to 49 mL of sterile Dulbecco's PBS pH 7.4. For the assay, 50 μL of the compound, at concentrations 0,5–0,001 mg/mL in PBS, were added to 950 μL of diluted blood. Immediately, after addition, the mixtures were continuously shaken on orbital shaker MaxQTM 6000 (Thermo Fisher Scientific TM, Rodano, MI, Italy) at 300 rpm, 37 °C for 2 h and thereafter further mixed by inversion every 15 min. After incubation, the mixtures were centrifuged at 503g for 5 min at 5 °C and the supernatants were analysed via UV-spectrometry at a wavelength of λ = 420 nm with a Tecan infinite M200 plate reader. Values were referred to 1 % Triton X-100 serving as 100 % reference value of haemolytic activity (positive control). The negative control was prepared by incubating 50 μL of sterile Dulbecco's PBS pH 7.4 and 950 μL of diluted blood. The extent of haemolysis as a percentage (% H) was determined by using the following equation:

$$\%\,Haemolysis = \frac{Abs\,Test - Abs\,Neg}{Abs\,Pos - Abs\,Neg} \times 100$$

where AbsTest is the absorbance of the test sample, AbsNeg is the absorbance of the negative control and AbsPos is the absorbance of the positive control (Lam et al., 2019).

#### 2.10.5. In vitro antitumor efficacy study

The *in vitro* cell viability assay was conducted as previously described (Iacobazzi et al., 2021). MGS and Hmel-1 cell lines were seeded at a density of 5,000 cells/well for 24 h in 96-well plates (Corning, NY, USA). Subsequently, the culture medium was replaced with 100 μL of fresh medium containing dilutions of free Cob and Lenva, and with the Cob and Lenva loaded in liposomes and hybrid liposomes. The cells were treated with the tested compounds at 37 °C for 24 h, then washed out and cultured in a fresh culture medium for a further 48 h. The tested concentration range was for Cob loaded or not, 0.1–1 μM on BRAF wild type MGS and 0.5–10 nM on Hmel-1 cell line, for Lenva loaded or not, 0.01–5 μM on both cell lines. Cell viability was assessed using MTT assay as previously described (Iacobazzi et al., 2021), and results were expressed as dose/effect plots of the mean of three different experiments at each tested dose or $IC_{50}$ values obtained using nonlinear regression in CalcuSyn v.1.1.1 software (Biosoft, Cambridge, UK).

### 2.11. Statistics

Results were expressed as the mean ± SD from three independent experiments and analysed using GraphPad Prism version 5.0 to calculate the significance between groups using paired *t*-test method and two-way analysis of variance (ANOVA) followed by the Bonferroni post hoc tests. Data are indicated with *p < 0.001 and *** p < 0.001.

## 3. Results and discussion

The production of NPs fused with CMs conventionally involves lipid fusion with CMs and repeated mechanical extrusion through nanoporous membranes. Sonication and extrusion cause disruptive forces that can shatter the structure of CMs and then fuse them with lipids to generate a biomimetic hybrid NP. These procedures require a lot of work and effort, and the characteristics of NPs can vary significantly from batch to batch. Powerful tools for the precise construction of biomimetic hybrid NPs have evolved in the form of microfluidic platforms that can integrate many different reaction chambers to control and tune the micromixing. However, the application of microfluidics to the production of NPs fused with CMs is limited by the difficulty of breaking CMs with simple hydrodynamic forces in microchannels. Implementing external force fields to microfluidic reaction channels is proposed as a solution to this problem. The concept of microfluidic sonication is to immerse a microfluidic device in an ultrasound bath before the start of the production process of biomimetic hybrids liposomes. In addition, the decision to use L-α-Phosphatidylcholine from soybean and cholesterol in our experiments was primarily motivated by their structural and functional roles in mimicking biological membranes. While it is true that these synthetic lipids do not possess specific characteristics to enhance cell interactions, they were selected for their biocompatibility and their ability to form stable lipid bilayers. The ratio between these two synthetic compounds was determined through a combination of literature research and preliminary experiments in order to optimize membrane stability and fluidity. We referred to (Rayamajhi et al., 2019) and to (Briuglia et al., 2015) assessing that the 2:1 ratio (70 % of lipids and 30 % of cholesterol) is the most suitable combination in terms of characterisation and as the most flexible formulation in order to permit the release of drugs with different physiochemical characteristics. Actually, our specific aim was to design a bio hybrid liposome that would interact with cell membranes solely based on the presence and properties of the target cell membranes (CMs). In this regard, the nature of the synthetic lipids (PC and cholesterol) played a crucial role in allowing us to focus on evaluating the influence of the CMs themselves on the internalization process, without any interference from the liposome components.

### 3.1. Cell membrane isolation, hybridization, and characterization

CMs were harvested from a metastatic melanoma cell line (MM) extracted from a patient biopsy material using the freeze–thaw process as described in the methods section. CMs were hybridized with synthetic liposomes using microfluidic technique. By preliminary investigations we identified 3:1 (aqueous-to-organic phase) flow rate ratio (FRR) and 4 mL/min total flow rate (TFR) as the best conditions for cell membrane incorporation.

Based on this, the first step in optimizing biomimetic hybrid liposomes consisted of tailoring mixing protocols to generate stable NPs in terms of average diameter, size homogeneity, and zeta potential. For this reason, the production of the biomimetic hybrid liposomes was performed by two different microfluidic devices manufactured by 3DP (Fig. 1) to evaluate how the geometry of the device could modify the formation of the hybrid liposomes in terms of size.

The possibility of effectively using the FDM 3D printing to produce microfluidic devices was already assessed (Sommonte et al., 2023b; Tiboni et al., 2021b). The developed zigzag device already described (Fig. 1, device 1), resulted effective to produce polymeric NPs (Tiboni et al., 2021b), liposomes (Zhang et al., 2023), and solid lipid NPs (Sommonte et al., 2023a). The potentiality of using 3DP in the development and production of microfluidic devices relies on the fact that it is possible for the researcher to personalize the device based on specific needs in a faster and more affordable way.

Microfluidic devices can be engineered to obtain passive micromixing with the aim to produce diverse types of nanocarriers without the need for any external energy source. While passive mixing relies only on the energy already present in the fluid flow, active mixing depends on the addition of an external source of energy to promote mixing, such as an electric field or ultrasonic one (Othman et al., 2015). Passive micromixers take advantage of the presence of internal structures that create perturbations in the microchannels. They can be splits, bas-relied, or other 3D structures that help to increase the contact surface and the contact time between the excipients and the drugs. Device 1 is characterized by a T-junction configuration, which is widely used due to its simplicity. In this device, two different channels meet at right angles, with the main channel carrying the continuous phase and the orthogonal channel providing the dispersed phase (Martins et al., 2018). The new device (Fig. 1, device 2) in this work, inherits the zigzag bas-relief from the already developed one (device 1), and is implemented by a new round mixing chamber presenting 3 cylinders in the middle that split and recombine the flow into it. Moreover, compared to the zigzag device used as a comparison (device 1), the inlets are developed to have a co-flow of the two fluids pumped into the chip. The inlets present a 1

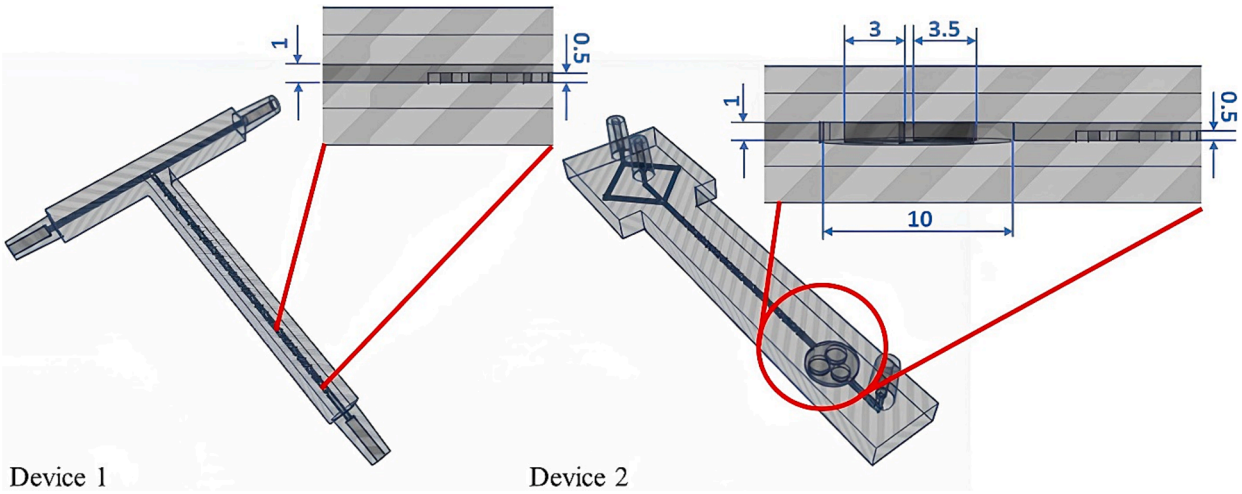


**Fig. 1.** Representative 3D models of the microfluidic devices employed. Dimensions are in mm.

mm square section while the zigzag structure has a height of 500 μm for both microfluidic devices (1 and 2). The new mixing chamber in device 2 has a diameter of 10 mm with the 3 internal cylinders having a diameter of 3 mm. The length of the zigzag structure is 50 mm. In this study, to best promote the breakdown of CMs and their fusion with synthetic lipids, we encouraged the combination of the two different ways to promote mixing, thus operating on both passive mixing driven by microfluidic device geometries and active mixing triggered by ultrasounds (Fig. 2).

Besides the employment of two different microfluidic geometries, the CMs were incorporated by increasing the protein-lipid ratio to generate stable hybrid liposomes in terms of membrane fusion, size homogeneity, and zeta potential. In the production of biomimetic hybrid liposomes, three different cell membrane concentrations were evaluated in terms of protein content, namely 66.4, 133.3, and 200 μg/mL producing respectively hybrid liposome@1, hybrid liposome@2, and hybrid liposome@3. As can be observed in Table 1, using both devices, 1 and 2, the incorporation of CMs at increasing protein concentrations (from 66.4 ($CMs_1$), 133.3 ($CMs_2$), to 200 μg/mL($CMs_3$)), induced a clear increase in the mean diameter of the resulting hybrid liposomes, i.e., using device 1 from 139.7 nm (control liposome) and 128.1 Ã· 137.1 (starting $CMs_{1-3}$ vesicles) to 145.2, 167.2, and 189.2 nm respectively, while a slight reduction of their surface charge is observed. Similarly, even using device 2 we observed a significant and gradual growth in size from 124.1 nm (control liposome) to 131.7, 145.6, and 151.9 nm, directly correlated with the amount of CMs employed. Reduction of the zeta potential of hybrid liposomes attributable to the fusion of CMs (ζ-potential $CMs_{1-3}$ = -18.8 Ã· − 20.8 mV) with the liposome (ζ-potential = -57.8 ± 1.57 mV) was also observed with microfluidic device 2 (Table 1). Specifically, we hypothesize that the negative zeta potential values observed in all samples can be attributed to the formulations with a 66:34 PC:Cholesterol molar ratio, which were prepared in DPBS with a specific ionic strength and pH 7.4. The zeta potential evaluation was conducted in bidistilled water with a pH around 5 to observe their surface properties without the influence of additional ions in the dispersant media.These results agree with what has been reported in the literature. *Rayamajhi et al.* suggest that the incorporation of CMs into the bilayer of synthetic liposomes enhances the water molecule's contact sites, increasing the hydration layers and, subsequently, the size of hybrid liposomes (Rayamajhi et al., 2019).

Furthermore, a noteworthy factor highlighted by the DLS analysis is that through device 2, much more homogeneously dispersed nanoparticle formulations were produced compared to device 1, as confirmed by the lower polydispersity index (PdI) values recorded. Employing device 1, hybrid liposome@2 and hybrid liposome@3 exhibited PdI values exceeding 0.3 indicating that the system was not monodisperse and probably the geometry and shorter length of the device did not provide efficient rupture and incorporation of CMs with lipids. Conversely, thanks to the geometry of device 2, biomimetic NPs with PdI lower than 0.2 were achieved suggesting high homogeneity in the size distribution and higher efficiency during the mixing (Table 1). This feature, in addition to the smaller nanoparticle sizes observed, leads to the conclusion that device 2 performed better, thanks to the enhanced mixing imparted by its geometry. With both microfluidic devices, the negativity of the hybrid liposomes decreased with increasing concentration of CMs, compared with liposome, attributed to the fusion of CMs with liposomes (Song et al., 2021).

FRET was performed to confirm the hybridization between liposome and CMs. FRET has been widely used to study membrane fusion. FRET liposomes were prepared with FRET pairs: PE-NB (Fluorescent donor, λem = 534 nm) PE-Rh-B (Fluorescent acceptor, λem = 595 nm) in 1:7 Molar ratio. Energy transfer in the FRET liposome was tracked before and after hybridization as illustrated in Fig. 3A. The liposome spectra represented the phase before hybridization, while the hybrid liposome

**Table 1**
Intensity average hydrodynamic diameter and corresponding PdI, determined by DLS, ζ-potential value of liposome and hybrid liposomes using different CMs protein content concentrations and two different microfluidic devices.

| Nanoformulations | $d_{mean}$ (nm) | Polydispersity Index (PdI) | ζ-potential (mV) |
|---|---|---|---|
| $CMs_1$ | 117.1 ± 1.0 | 0.202 ± 0.037 | −18.8 ± 1.19 |
| $CMs_2$ | 124.3 ± 2.3 | 0.221 ± 0.027 | −19.2 ± 2.28 |
| $CMs_3$ | 137.1 ± 2.1 | 0.214 ± 0.064 | −20.8 ± 2.10 |
| Liposome device 1 | 139.7 ± 3.0 | 0.208 ± 0.062 | −62.3 ± 2.29 |
| Hybrid liposome@1 device 1 | 145.2 ± 7.6 | 0.204 ± 0.089 | −60.8 ± 1.79 |
| Hybrid liposome@2 device 1 | 167.2 ± 3.5 | 0.345 ± 0.076 | −59.3 ± 2.18 |
| Hybrid liposome@3 device 1 | 189.2 ± 5.2 | 0.438 ± 0.031 | −57.9 ± 1.89 |
| Liposome device 2 | 124.1 ± 2.0 | 0.168 ± 0.035 | −57.8 ± 1.57 |
| Hybrid liposome@1 device 2 | 131.7 ± 5.9 | 0.122 ± 0.011 | −52.6 ± 1.82 |
| Hybrid liposome@2 device 2 | 145.6 ± 3.6 | 0.156 ± 0.034 | −49.7 ± 1.28 |
| Hybrid liposome@3 device 2 | 151.9 ± 2.4 | 0.181 ± 0.045 | −46.6 ± 1.40 |

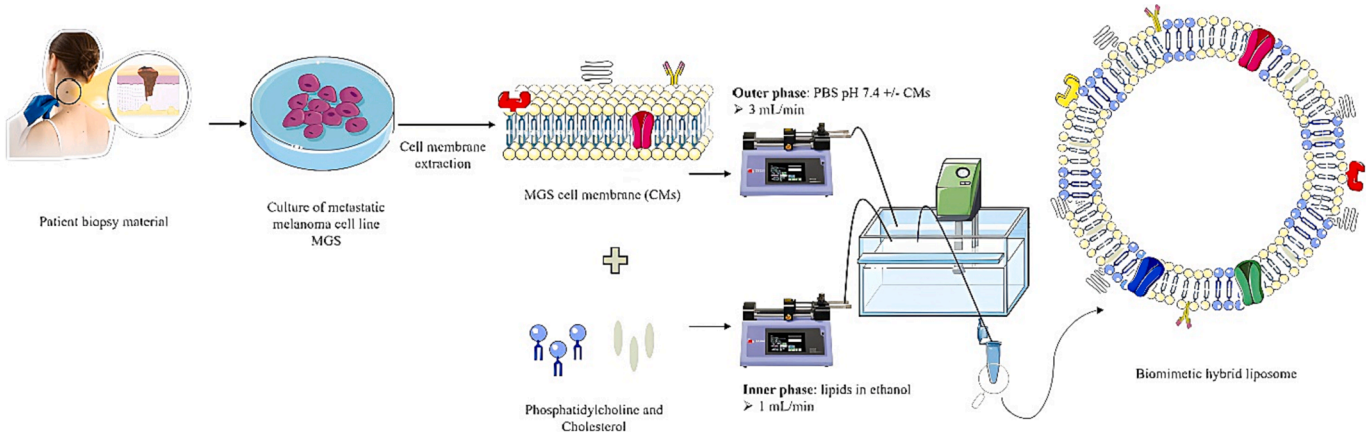


**Fig. 2.** Schematic representation of the fabrication of hybrid liposome. In detail, the cell membranes derived from the BRAF wild-type metastatic melanoma cell line (MGS) and extracted from a patient's biopsy material were mixed with phospholipids and cholesterol inside the microfluidic device. Mixing was facilitated by incorporating external force fields into the microfluidic platform.

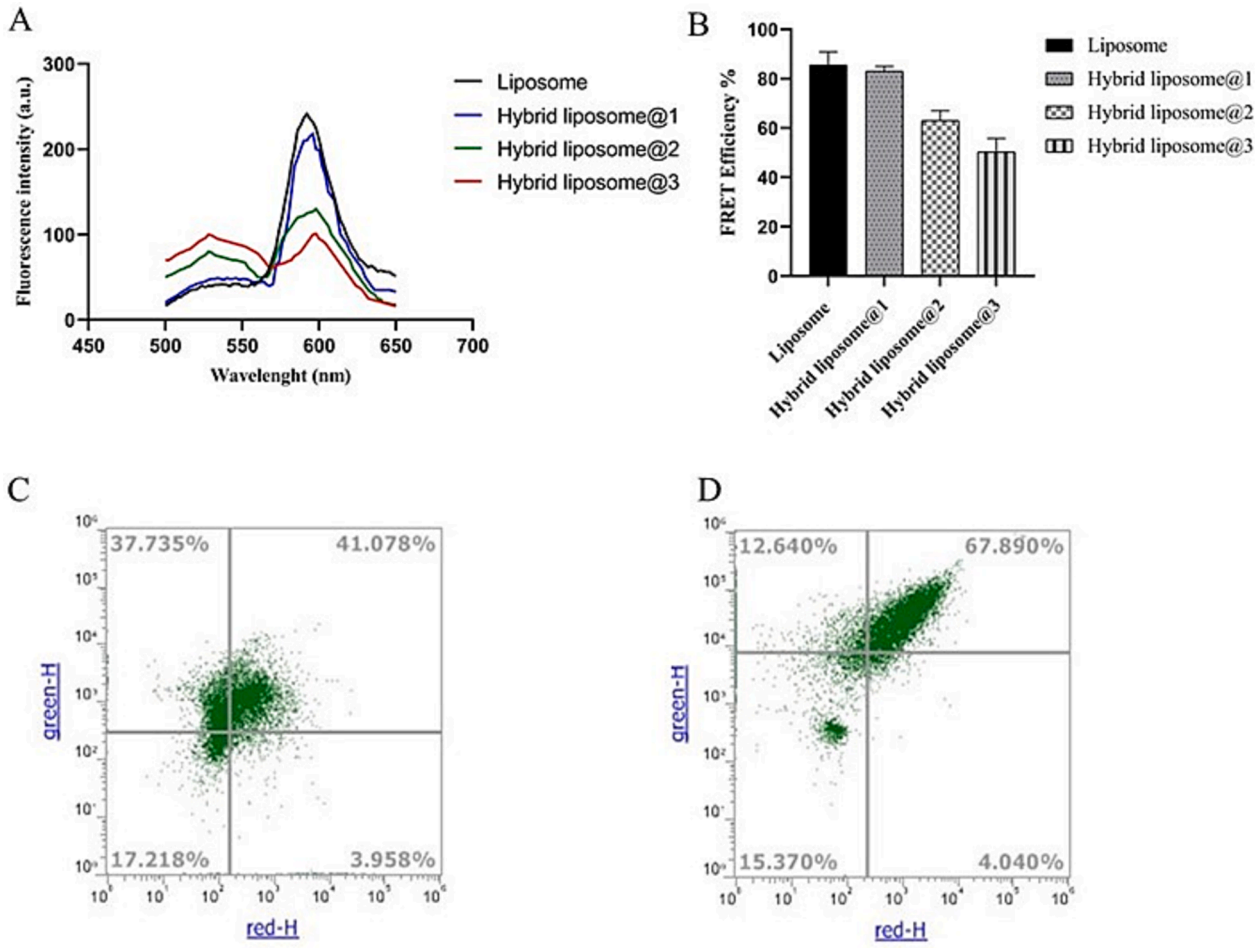


**Fig. 3.** Validation of hybrid liposome formation. (A) FRET study showing successful hybridization of CMs and liposome. FRET study was conducted using fluorescent donor NBD (λem = 525 nm) and fluorescent acceptor RhB (λm = 595 nm) at excitation wavelength of 470 nm. (B) Quantification of FRET efficiency and decrement of FRET efficiency after hybridization with increasing amounts of CMs. All bars represent means ± s.d; n = 3. (C and D) Validation of liposome-CMs fusion by flow cytometry analysis by calculating the % of NPs in which red and green fluorescence colocalized for hybrid liposome@2 (C) and hybrid liposome@3 (D). (For interpretation of the references to colour in this figure legend, the reader is referred to the web version of this article.)

spectra displayed the phase after hybridization. The FRET effect was detected after hybridization, which can only occur when the distance between FRET pairs increases. This suggested that there was an incorporation of CM content into the lipid bilayer of the liposome, validating the success of hybridization. To quantify the diminished FRET effect, FRET efficiency was calculated. Fig. 3B displayed a decay in FRET efficiency in hybrid liposomes as the amount of CMs increased. Specifically, for the hybrid liposome@2, we found a decrease of about 20 % while for the hybrid liposome@3 a decrease of 35 %.

Moreover, the fusion of the lipid membrane and CMs in hybrid liposomes@2 and hybrid liposomes@3 were displayed by FCM analysis by marking the lipid membrane and CMs with green, fluorescent dye PKH67 and red fluorescent dye PKH26, respectively. As can be observed from Fig. 3C and 3D in the case of hybrid liposome@2 the % of NPs for which red and green were colocalized was about 40 % while for hybrid liposomes@3 the % of NPs with green and red fluorescence colocalization, increased to about 68 %. Considering the experiments carried out for hybridization validation, excluding the hybrid liposome@1 preparation in which the low concentration of CMs did not permit us to demonstrate an effective validation by FRET analysis, for the other two preparations, hybrid liposomes@2, and hybrid liposomes@3 FRET analysis allowed us to confirm an effective fusion, with improved achievement for the hybrid liposome@3 formulation (Fig. 3A). These finding were validated by co-localization analysis by FCM (Fig. 3C and 3D). For these reasons, subsequent analyses were conducted on the hybrid liposome@3 and liposome employing microfluidic device 2.

After optimizing the production procedure and identifying the optimal amount of CMs for hybrid liposome formation, the hybrid liposome@3 formulation was manufactured by incorporating a fluorescent lipid for *in vitro* uptake studies (Fig. 4A). The formulation hybrid liposome@3 has been further analyzed using NTA for a more accurate analysis of the size distribution and to obtain information about the concentration of NPs. The data of the NTA was in agreement with those reflected by the DLS analysis (Fig. 4A-B). In addition, the liposome concentration was reported to be 2.4 x $10^9$ particle/mL comparable to the hybrid@3 liposome concentration of 2.8 x $10^9$ particle/mL. Thus, the similar number of NPs in the two preparations, suggested that the size increase obtained for hybrid liposomes is indeed related to the intermixing of CMs among lipids, and not to the aggregation of hybrid NPs. Liposomes and hybrid liposomes were further characterized by transmission electron microscopy (TEM) to study the morphological characteristic. TEM images (Fig. 4C) displayed morphological features of these NPs at lower and higher magnifications. Lower magnification images demonstrated a general distribution of NPs with spherical structures. Higher magnification images of liposome and hybrid liposome showed NPs with similar sizes (around 80 nm in the dry state).

### 3.2. *Cobimetinib and lenvatinib loading and release studies*

Later on, we explored drug loading and release studies to investigate

A

| | DLS | | | NTA* | |
|---|---|---|---|---|---|
| Nanoformulation | $d_{mean}$ (nm) | Polydispersity Index (PdI) | ζ-potential (mV) | Mode (nm) | Particle/mL |
| Liposome device 2 | 124.1 ±2.0 | 0.168 ±0.035 | -57.8 ±1.63 | 136.1±1.1 | 2.4 x $10^9$ |
| Hybrid Liposome@3 device 2 | 151.9 ±2.4 | 0.181 ±0.045 | -46.6 ±1.45 | 167.6±2.1 | 2.8x$10^9$ |
| Fluo* Liposome device 2 | 114 .0 ±1.3 | 0.195 ±0.023 | -56.1 ±6.96 | - | - |
| Fluo* Hybrid Liposome@3 device 2 | 189.2 ±4.5 | 0.257 ±0.018 | -53.0 ±0.47 | - | - |

*Concentration (particle/mL and size distribution (mode,nm) determinated by NTA (Nanoparticle Tracking analysis)

*1,2-dipalmitoyl-sn-glycero-3-phosphoethanolamine-N-(lissamine rhodamine B sulfonyl)

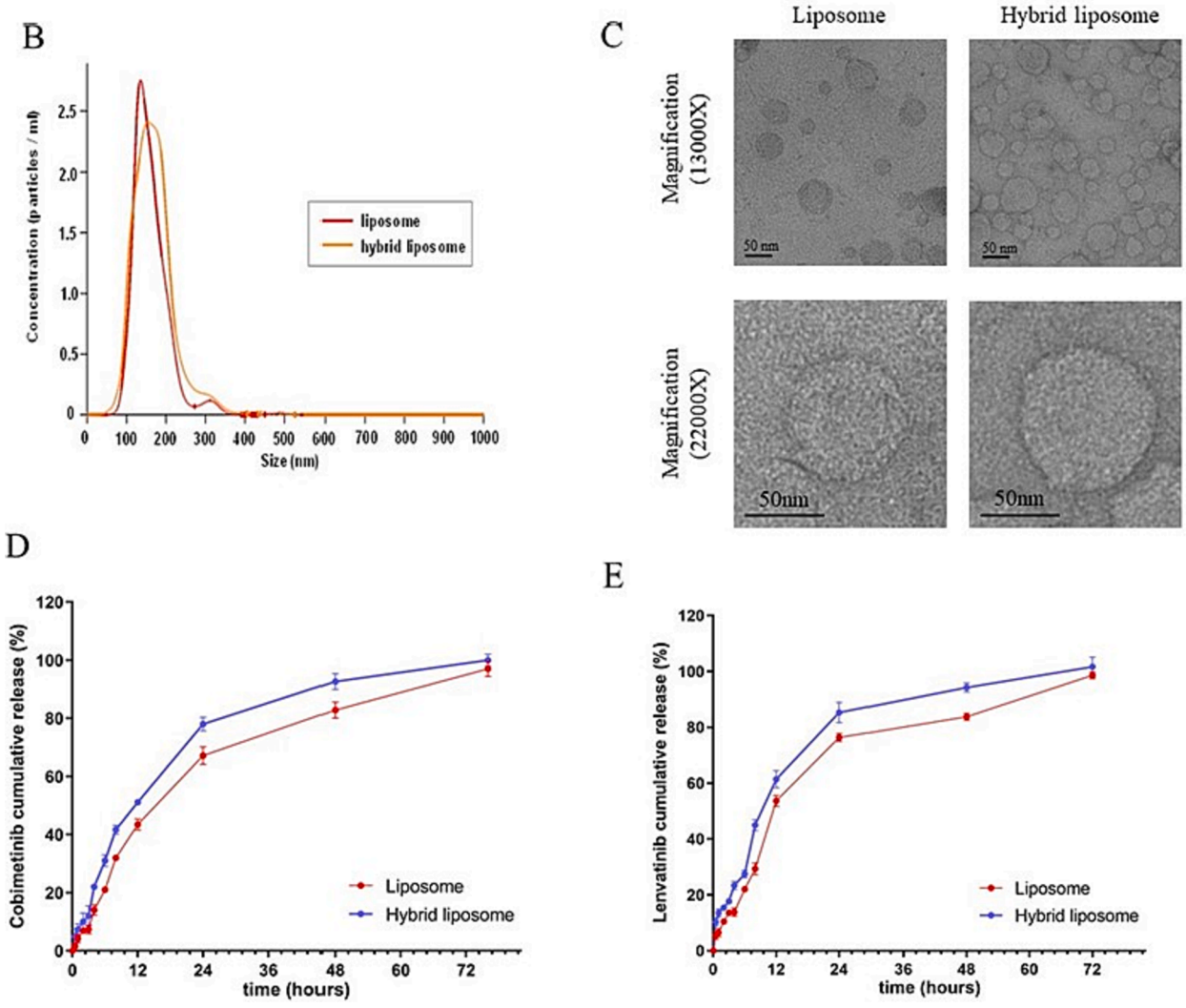


**Fig. 4.** (A) Intensity-average hydrodynamic diameter and corresponding polydispersity index (PdI) determined by DLS and ζ-potential of liposome and hybrid liposome@3 produced through microfluidic device 2. (A and B) Concentration and size distribution of liposomes and hybrid liposome@3 determined by NTA. (C) TEM images of liposome and hybrid liposome at different magnifications. (D and E) In vitro release profiles of cobimetinib (D) and lenvatinib (E) from liposome and hybrid liposome in PBS at 37 °C at pH 7.4. Results are reported as mean ± SD, n = 3.

the potential application of biomimetic hybrid liposomes in drug delivery. Cob and Lenva were loaded into the hybrid liposome separately, and liposome Cob and liposome Lenva were used as control. High encapsulation efficiencies were obtained for both drugs in both the conventional liposomal nanosystem and the biomimetic hybrid liposome. Specifically for both drugs, the EE % in the hybrid liposome exceeded 70 % (Table 2). The *in vitro* release studies were conducted as reported in the literature (Iacobazzi et al., 2021; Sommonte et al., 2023a). The Cob and Lenva release from the liposome and hybrid liposome was explored at normal physiological pH 7.4 as depicted in

**Table 2**
Intensity average hydrodynamic diameter and corresponding PdI, determined by DLS, ζ-potential value, and drug encapsulation efficiency (EE%) of drug-loaded hybrid liposome.

| Nanoformulation | $d_{mean}$ (nm) | Polydispersity Index (PdI) | ζ-potential (mV) | Encapsulation Efficiency (%) |
|---|---|---|---|---|
| Liposome-Cob | 116.4 ± 2.5 | 0.183 ± 0.020 | −67.2 ± 2.27 | 62.15 ± 1.78 |
| Hybrid Liposome Cob | 174.0 ± 3.5 | 0.259 ± 0.027 | −55.7 ± 1.46 | 77.65 ± 3.98 |
| Liposome Lenva | 137.5 ± 3.9 | 0.110 ± 0.023 | −67.2 ± 2.27 | 73.67 ± 5.34 |
| Hybrid Liposome Lenva | 167.9 ± 1.2 | 0.189 ± 0.039 | −55.7 ± 1.46 | 75.38 ± 6.26 |

Fig. 4D and 4E. For both drugs, the hybrid liposomes displayed an sustained release up to 72 h. The release of Cob and Lenva from the liposomes (used as control) exhibited similar release characteristics with those from the hybrid liposome, with a sustained release.

### 3.3. Cellular uptake studies

To test whether hybrid liposomes exhibited self-recognition on the corresponding homologous cell line (MGS) and increased cellular internalization, we performed uptake studies on both MGS and Hmel-1 cell lines and on the hepatocarcinoma-derived cell line SK-HEP-1. As evidenced in histograms A and B and in Table C of Fig. 5, a marked increase in the amount of internalized fluorescence was observed for hybrid liposomes compared with liposomes, in all cell lines. This was more evident in MGS cells than in SK-HEP-1 cells. Moreover, among melanoma cell lines, a significantly higher internalized fluorescence was observed in MGS cells. This was also evidenced by the ratio of internalized hybrids/liposomes (8 ± 0.5 for MGS, 2.1 ± 0.1 for Hmel-1, and 1.9 ± 0.1 for SK-HEP-1 (Fig. 5 B, C). Taken together, these results highlighted the homotypic targeting ability of MGS-hybrid liposomes, which was also confirmed by the results on the investigation of internalized fluorescence intensity (FI) performed in MGS 3D model. In fact, a greater fluorescence intensity was observed for the hybrid liposomes compared to the liposomes (Fig. 5 D). In particular, the colocalized rhodamine/hoechst fluorescences measured in pixel count were NP = 153 ± 20 and NP = 60 ± 15, for hybrid liposomes and liposomes, respectively. Thus, the FI investigation was consistent with FCM analysis, demonstrating the efficacy of homotypic targeting to promote increased cell internalization.

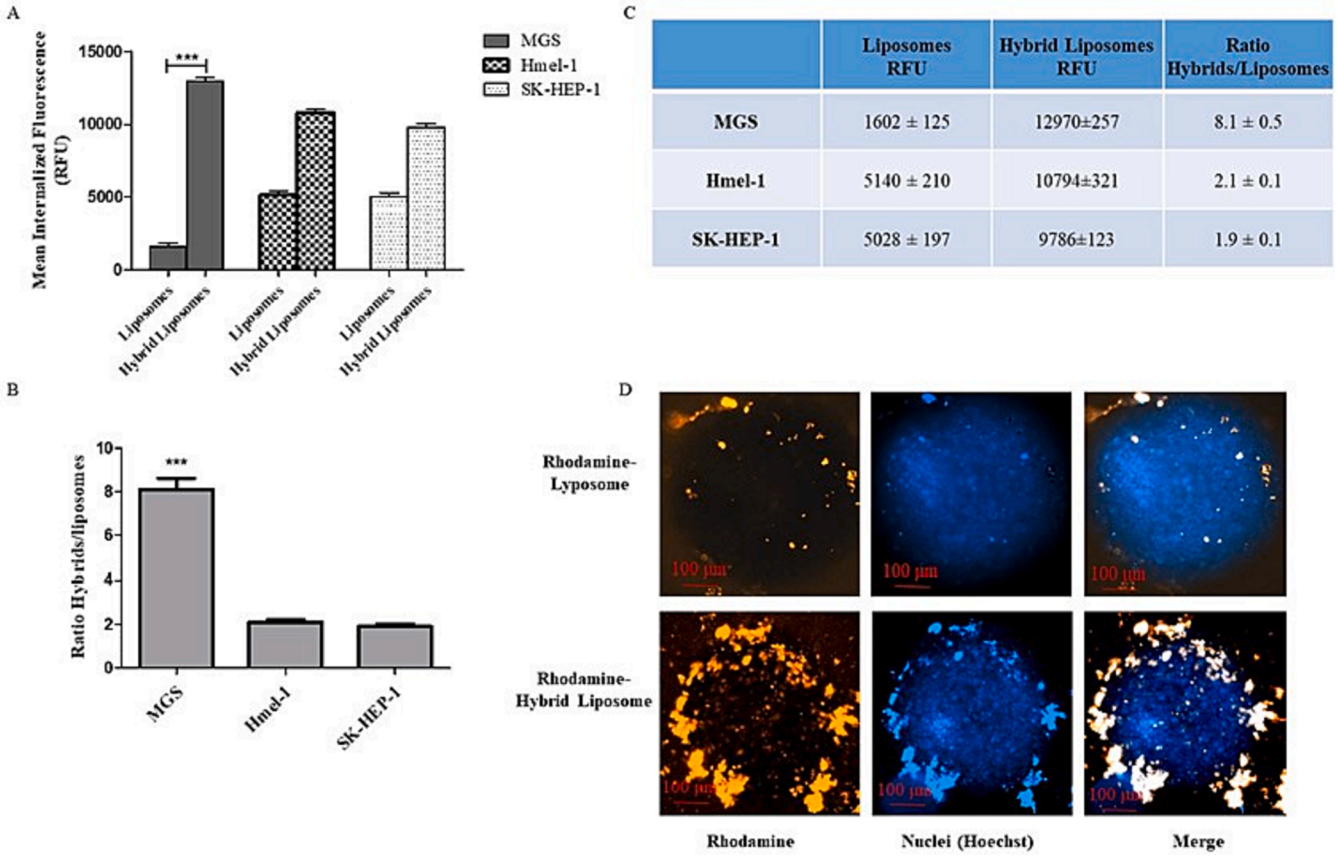


**Fig. 5.** (A-C) Uptake experiment results by Flow-cytometry analysis. (A) Average internalized fluorescence values (37°- 4° values) expressed in relative fluorescence units (RFU) of liposome and Hybrid Liposomes tested at 1 μM concentration in terms of fluorescent lipids.. (B) Ratio of Hybrid liposome/Liposomes mean internalized fluorescence values. A difference was considered to be very significant with *** $p < 0.0001$. (C) Mean internalized fluorescence values (37°- 4° values) expressed in RFU. (D) Representative images showing cell uptake of fluorescent NPs in 3D MGS model. The upper panel shows the fluorescence intensities of Rhod-Liposomes (orange), Hoechst (blue, nuclei), and the merge of them; the bottom panel shows the fluorescence intensities of Rhod-Hybrid Liposomes (orange), Hoechst (blue, nuclei), and merge of them. Scale bar 100 μm. (For interpretation of the references to colour in this figure legend, the reader is referred to the web version of this article.)

### 3.4. Endocytic entry mechanism study

The ability of a drug to have a therapeutic effect at its site of action is regulated by the NPs' ability to enter the cell. Internalization routes are not ubiquitary. Phagocytosis and macropinocytosis, for instance, are not specific for all cell types. Nevertheless, there is less evidence that other commonly studied internalization pathways are also restricted to some cells. Thus, it is crucial to understand whether the pathways studied are present in cells when studying NPs uptake (Rennick et al., 2021). Establishing the mechanism of uptake can provide important information on release efficiency, therapeutic activity, and translation to other cells or *in vivo* studies. Two main routes of entry into the cell exist: direct fusion with the plasma membrane or endocytosis. However, the main route of entry of NPs into the cell is endocytosis. Currently, there is a growing acceptance of five main types of endocytosis: (1) clathrin-coated pit-mediated endocytosis, (2) fast endophilin-mediated endocytosis, (3) clathrin-independent carrier, (4) macropinocytosis, (5) phagocytosis, and (6) caveolae mediated internalization, which in theory can also contribute to endocytic uptake. There is also a clear cross-talk between pathways and also, inhibition of one pathway can modulate another and therefore compensate for the lack of that pathway (Rennick et al., 2021).

Based on the results of the uptake experiments conducted at 4 °C (Fig. 6A) which showed a significant inhibition of hybrid liposomes and liposomes internalization in MGS cells, for these type of NPs we suggested an energy-dependent endocytosis process. The energy-dependent endocytosis is likely to be a result of a combination of factors, including protein activity and membrane fluidity. It is well-established that cellular processes like endocytosis are often energy-dependent due to the involvement of various ATP-driven processes, such as membrane deformation and vesicle trafficking. Additionally, protein activity, particularly that of membrane receptors and associated signaling pathways, could play a significant role in regulating this process (Rennick et al., 2021). Thus, to know whether a specific pathway of endocytosis was involved, we performed uptake experiments using LY294002, as inhibitor of micropinocytosis, potassium depletion buffer (K + DB, isotonic), as inhibitor of the clathrin-mediated endocytosis, and methyl-β-cyclodextrin, as inhibitor of the Clathrin-independent endocytosis. As shown in Fig. 6 B, a marginal reduction in cell-associated fluorescence was observed, referred to cell-associated fluorescence of NPs in absence of inhibitor (3.0 ± 0. 5 % and 1.0 ± 0.2 % for hybrid liposomes and liposomes, respectively), only following potassium depletion buffer inhibition. Thus, according to the theory above mentioned that inhibition of one pathway can modulate another and so compensate for the lack of that pathway, we suggest that no specific endocytosis mechanism was involved for hybrid liposomes and liposomes.

### 3.5. Haemolysis test

The haemolytic activity of drug delivery systems is a simple and reliable measure for estimating cell membrane damage caused by formulations *in vivo*. This test is of prime importance for parenteral drug delivery systems to determine their compatibility with blood components. The haemolytic activity of different concentrations of the nanoformulations is shown in Fig. 7. The haemolytic activity of hybrid liposomes and liposomes in the concentration range investigated was very low and comparable to the negative control PBS.

### 3.6. Antitumor efficacy studies

As reported before, the anti-tumor activity of liposomes and hybrid liposomes with the encapsulated targeted agents Cob and Lenva was tested on both MGS and Hmel-1 cell lines. The choice of these two drugs relies on different aspects, such as the optimization of current therapies and the search for new treatment options especially for BRAF wild type melanoma. Indeed Lenva is a multi-targeted tyrosine kinase inhibitor (TKI) that targets several cancer-associated pathways, already tested in melanoma with little benefit but recently showing promising results in combination with immunotherapies (Stoff et al., 2023) and to date cobimetinib has been used successfully in BRAFV600E MM (Ascierto et al., 2023). Therefore, we investigated the possible advantage of using hybrids liposomes to improve the efficacy of both drugs either in BRAF wild type and BRAFV600 mutant MM model. The empty liposomes and hybrid liposomes were also tested to understand the intrinsic cytotoxicity of the carrier, which showed no cytotoxic effect in the range of concentrations investigated (data not shown).

The dose/effect curves shown in the Fig. 8compare the antitumor activity of the free drug, liposome-encapsulated, and hybrid liposome-encapsulated. Both curves referring to the preparations with Cob and Lenva (Fig. 8 A and B), and the table in the Fig. 8 C, suggest that the cytotoxic concentration of the drug-loaded nanosystems expressed as $IC_{50}$, is lower than that of the free drug (Cob: 0.09 ± 0.03 μM and 0.18 ± 0.10, for MGS and Hmel-1, respectively; Lenva: 1148 ± 20 and 10247 ± 210, for MGS and Hmel-1, respectively). Specifically, for MGS the $IC_{50}$ of the hybrid liposomes is lower than that of the liposome (0.06 ± 0.01 μM and 0.08 ± 0.02 μM for the Cob Hybrid liposomes and liposomes, respectively; 7 ± 2 and 9 ± 1 μM for Lenva loaded hybrid liposome and liposomes, respectively). This means that lower concentrations of the hybrid liposome system are able to inhibit the proliferation of at least 50 % of cancer cells, making it a more potent system than the others. The same comparison can be seen from the dose/effect graph referring to the cytotoxic activity of hybrid liposomes and liposomes in Hmel-1 cells. Another deduction we can make concerns the use of Cob in therapy. As previously mentioned, this drug is commonly used in the treatment of

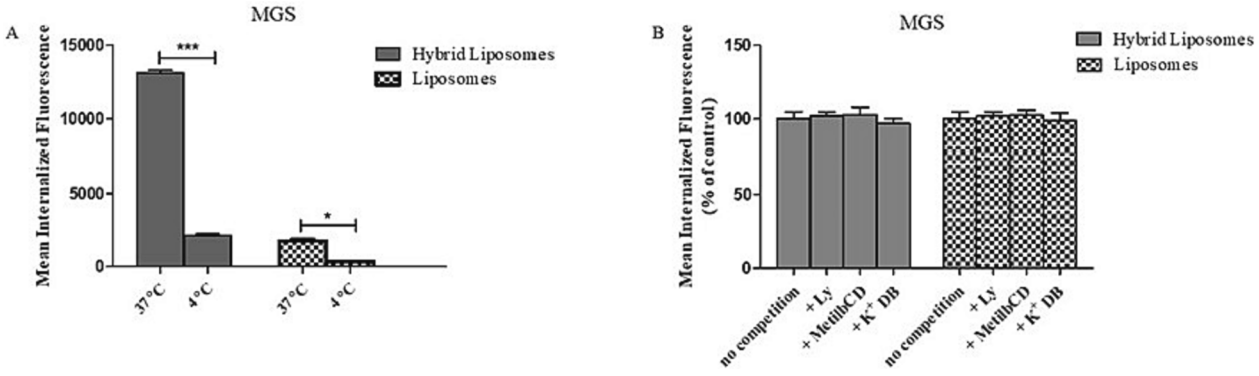


**Fig. 6.** Effect of temperature (A) and of endocytosis inhibitors (B), on accumulation of hybrid liposomes and liposomes in MGS cells. Results are expressed as mean of internalized fluorescence at 37 °C and 4 °C in (A), and relative to cell-associated fluorescence of hybrid liposomes or liposomes used as control, in the absence of inhibitor. A difference was considered to be very significant with *** $p < 0.0001$ and significant with * $p < 0.01$. Data represent mean ± SD, n = 3.

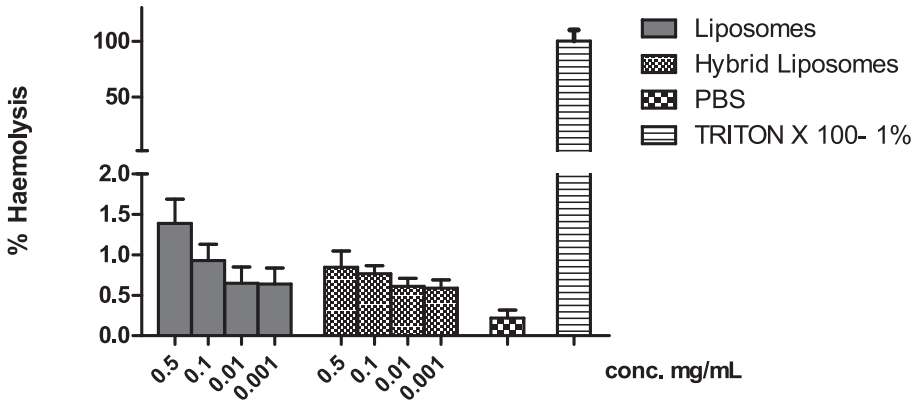


**Fig. 7.** *In-vitro* red blood cell haemolysis of Hybrid liposomes and liposomes at 0.001–0.5 mg/mL concentration. Data are shown as mean ± SD (n = 3).

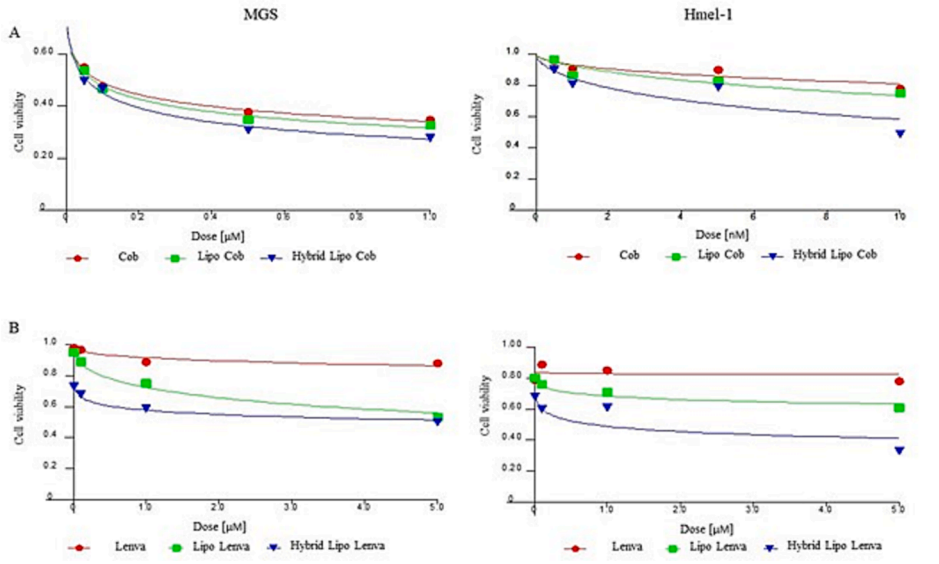


C

| | $IC_{50}$ μM | |
|---|---|---|
| Samples | MGS | Hmel-1 |
| Cobimetinib | 0.09 ± 0.03 | 0.18 ± 0.1 |
| Liposome Cob | 0.08 ± 0.02 | 0.05 ± 0.01 |
| Hybrid Liposome Cob | 0.06 ± 0.01 | 0.02 ± 0.01 |
| Lenvatinib | 1148 ± 20 | 10247 ± 210 |
| Liposome Lenvatinib | 9 ± 1 | 226 ± 12 |
| Hybrid Liposome Lenva | 7 ± 2 | 0.83 ± 0.22 |

**Fig. 8.** (A, B) Dose/effect plots of the mean of three different cell viability experiments, conducted in MGS and Hmel-1 cell lines incubated for 24 h + 48 h w.o. with free Cob, Liposome Cob and Hybrid Liposome Cob (Panel A) or Lenva, Liposome Lenva and Hybrid Liposome Lenva (Panel B). (C) $IC_{50}$ values of MGS and Hmel-1 cell lines treated with all treatment conditions; the data are reported as the mean of three independent experiments.

BRAFV600 mutant metastatic melanoma; however, we tested the antiproliferative activity of the molecule in BRAF wild-type MGS cells, thus not presenting the mutation. Having obtained good cytotoxicity results, we can assume that the drug may also be useful in the therapy of BRAF wild type metastatic melanoma, but further investigations will be needed. Regarding Lenva, it is evident that its encapsulation in hybrid liposomes, especially if we refer to Hmel-1 cells, led to a significant reduction in $IC_{50}$ and thus a significant increase in antitumor efficacy compared with the free drug. Certainly, one reason to ascribe the greater efficacy of the encapsulated drug over the free drug lies in the sustained drug release kinetics, highlighted by purposely performing the *in vitro* cytotoxicity studies by incubating the cells with the compounds for 24 h and then operating the wash out by continuing the experiment for 48 h. This is particularly evident for Lenva, which normally has anti-angiogenic characteristics, and instead when encapsulated turns out to be cytotoxic.

These results suggest to us to explore more thoroughly in order to translate the use of hybrid liposome into the therapy of both wild type and mutated metastatic melanomas. However, we feel that the innovation of this study is the design of production process by microfluidics.

## 4. Conclusions

The innovation of this study is the design of a customized, flexible and efficient microfluidic platform to produce biomimetic hybrid liposomes. The intricate internal geometric architecture of both microfluidic devices allowed for an adequate degree of passive mixing of the two phases, which combined with the active mixing promoted by ultrasounds, produced high-quality monodisperse hybrid liposomes. The hybrid liposomes mirrored the membrane composition of MGS cells and inherited the multivalent targeting functionality with the highest concentration of CMs. Meanwhile, hybrid liposome exhibited excellent physicochemical properties, high drug loading capacity, sustained drug release profile and good tolerability. 2D and 3D *in vitro* uptake studies showed that the hybrid liposomes had a stronger affinity for its source MGS cancer cells than conventional liposomes, hence exhibiting a capacity for homotypic targeting and internalization via an energy dependent endocytosis process. Moreover, to consider this biomimetic nanosystem as a potential therapeutic tool for the personalized treatment of metastatic melanoma, Cob and Lenva, were efficiently loaded, demonstrating an *in vitro* higher antitumor efficacy referred to the free drugs administration. Notably, the hybrid liposomes showed negligible toxicity as demonstrated by bona fide haemolysis test. Collectively our results demonstrated that this biomimetic nanosystem, with the

potential of large-scale production and for downstream translation, is a promising tool for optimizing the therapeutic potential of current drugs and ultimately for improving efficacy and approaches for the treatment of MM. In conclusion, the approach we have demonstrated here, has the advantage of potential versatility in using cell membranes extracted from different cell sources and thus from biopsy samples collected from different patients. The final aspect, while warranting additional investigation, is essential in the context of personalized therapy, particularly for patients with metastatic melanoma, as examined in the current study. Furthermore, the implications go beyond this specific case to encompass a broader range of therapeutic disciplines.

**Authors' information:** the authors affiliated to the IRCCS Istituto Tumori Giovanni Paolo II are responsible for the views expressed in this article, which do not necessarily represent the ones of the Institute.

## CRediT authorship contribution statement

**Ilaria Arduino:** Investigation, Methodology, Writing – original draft, Writing – review & editing. **Roberta Di Fonte:** Data curation, Investigation, Writing – original draft. **Mattia Tiboni:** . **Letizia Porcelli:** Formal analysis, Writing – review & editing. **Simona Serratì:** Investigation. **Dafina Fondaj:** Investigation. **Tania Rafaschieri:** Investigation. **Annalisa Cutrignelli:** Data curation, Formal analysis. **Gabriella Guida:** Resources. **Luca Casettari:** Investigation, Resources. **Amalia Azzariti:** Conceptualization, Supervision, Writing – review & editing. **Angela Assunta Lopedota:** Data curation, Writing – review & editing. **Nunzio Denora:** Conceptualization, Data curation, Writing – review & editing. **Rosa Maria Iacobazzi:** Conceptualization, Project administration, Writing – original draft, Supervision, Writing – review & editing.

## Declaration of competing interest

The authors declare that they have no known competing financial interests or personal relationships that could have appeared to influence the work reported in this paper.

## Data availability

No data was used for the research described in the article.

## Acknowledgments

We thank: M.I.U.R.—Programma Operativo Nazionale (PON) "Ricerca e Innovazione" 2014–2020 Tematica IV.4 "Dottorati e Contratti di ricerca su tematiche dell'innovazione", MUR- National Center for Gene Therapy and Drugs based on RNA Technology (CN00000041)-Spoke 1- Piano Nazionale di Ripresa e Resilienza (PNRR), Missione 4, Componente 2, Investimento 1.4 "Potenziamento strutture di ricerca e creazione di "campioni nazionali di R&S"- NextGenerationEU and, European Union - NextGenerationEU under the Italian Ministry of University and Research (MUR) National Innovation Ecosystem grant ECS00000041 - VITALITY - CUP H33C22000430006.

## References

Abreu, C.M., Costa-Silva, B., Reis, R.L., Kundu, S.C., Caballero, D., 2022. Microfluidic platforms for extracellular vesicle isolation, analysis and therapy in cancer. Lab Chip 22, 1093–1125. https://doi.org/10.1039/d2lc00006g.

Arduino, I., Depalo, N., Re, F., Dal Magro, R., Panniello, A., Margiotta, N., Fanizza, E., Lopalco, A., Laquintana, V., Cutrignelli, A., Lopedota, A.A., Franco, M., Denora, N., 2020. PEGylated solid lipid nanoparticles for brain delivery of lipophilic kiteplatin Pt (IV) prodrugs: an in vitro study. Int. J. Pharm. 583, 119351 https://doi.org/10.1016/j.ijpharm.2020.119351.

Arduino, I., Liu, Z., Iacobazzi, R.M., Lopedota, A.A., Lopalco, A., Cutrignelli, A., Laquintana, V., Porcelli, L., Azzariti, A., Franco, M., Santos, H.A., Denora, N., 2021. Microfluidic preparation and in vitro evaluation of iRGD-functionalized solid lipid nanoparticles for targeted delivery of paclitaxel to tumor cells. Int. J. Pharm. 610, 121246 https://doi.org/10.1016/j.ijpharm.2021.121246.

Ascierto, P.A., Agarwala, S.S., Warner, A.B., Ernstoff, M.S., Fox, B.A., Gajewski, T.F., Galon, J., Garbe, C., Gastman, B.R., Gershenwald, J.E., Kalinski, P., Krogsgaard, M., Leidner, R.S., Lo, R.S., Menzies, A.M., Michielin, O., Poulikakos, P.I., Weber, J.S., Caracò, C., Osman, I., Puzanov, I., Thurin, M., 2023. Perspectives in Melanoma: meeting report from the Melanoma Bridge (December 1st–3rd, 2022—Naples, Italy). J. Transl. Med. 21, 508. https://doi.org/10.1186/s12967-023-04325-x.

Briuglia, M.-L., Rotella, C., McFarlane, A., Lamprou, D.A., 2015. Influence of cholesterol on liposome stability and on in vitro drug release. Drug Deliv. Transl. Res. 5, 231–242. https://doi.org/10.1007/s13346-015-0220-8.

Chen, J., Tan, Q., Yang, Z., Jin, Y., 2022. Engineered extracellular vesicles: potentials in cancer combination therapy. J Nanobiotechnology 20. https://doi.org/10.1186/s12951-022-01330-y.

Chen, Z., Zhao, P., Luo, Z., Zheng, M., Tian, H., Gong, P., Gao, G., Pan, H., Liu, L., Ma, A., Cui, H., Ma, Y., Cai, L., 2016. Cancer Cell Membrane-Biomimetic Nanoparticles for Homologous-Targeting Dual-Modal Imaging and Photothermal Therapy. ACS Nano 10, 10049–10057. https://doi.org/10.1021/acsnano.6b04695.

Denora, N., Laquintana, V., Lopalco, A., Iacobazzi, R.M., Lopedota, A., Cutrignelli, A., Iacobellis, G., Annese, C., Cascione, M., Leporatti, S., Franco, M., 2013. In vitro targeting and imaging the translocator protein TSPO 18-kDa through G(4)-PAMAM–FITC labeled dendrimer. J. Control. Release 172, 1111–1125. https://doi.org/10.1016/j.jconrel.2013.09.024.

Fang, R.H., Hu, C.-M.-J., Luk, B.T., Gao, W., Copp, J.A., Tai, Y., O'Connor, D.E., Zhang, L., 2014. Cancer Cell Membrane-Coated Nanoparticles for Anticancer Vaccination and Drug Delivery. Nano Lett. 14, 2181–2188. https://doi.org/10.1021/nl500618u.

Fondaj, D., Arduino, I., Lopedota, A.A., Denora, N., Iacobazzi, R.M., 2023. Exploring the Microfluidic Production of Biomimetic Hybrid Nanoparticles and Their Pharmaceutical Applications. Pharmaceutics 15, 1953. https://doi.org/10.3390/pharmaceutics15071953.

He, Y., Li, R., Li, H., Zhang, S., Dai, W., Wu, Q., Jiang, L., Zheng, Z., Shen, S., Chen, X., Zhu, Y., Wang, J., Pang, Z., 2019. Erythroliposomes: Integrated Hybrid Nanovesicles Composed of Erythrocyte Membranes and Artificial Lipid Membranes for Pore-Forming Toxin Clearance. ACS Nano 13, 4148–4159. https://doi.org/10.1021/acsnano.8b08964.

Himbert, S., Gastaldo, I.P., Ahmed, R., Pomier, K.M., Cowbrough, B., Jahagirdar, D., Ros, S., Juhasz, J., Stöver, H.D.H., Ortega, J., Melacini, G., Bowdish, D.M.E., Rheinstädter, M.C., 2022. Erythro-VLPs: Anchoring SARS-CoV-2 spike proteins in erythrocyte liposomes. PLoS One 17. https://doi.org/10.1371/journal.pone.0263671.

Hu, C.-M.-J., Fang, R.H., Wang, K.-C., Luk, B.T., Thamphiwatana, S., Dehaini, D., Nguyen, P., Angsantikul, P., Wen, C.H., Kroll, A.V., Carpenter, C., Ramesh, M., Qu, V., Patel, S.H., Zhu, J., Shi, W., Hofman, F.M., Chen, T.C., Gao, W., Zhang, K., Chien, S., Zhang, L., 2015. Nanoparticle biointerfacing by platelet membrane cloaking. Nature 526, 118–121. https://doi.org/10.1038/nature15373.

Iacobazzi, R.M., Porcelli, L., Lopedota, A.A., Laquintana, V., Lopalco, A., Cutrignelli, A., Altamura, E., Di Fonte, R., Azzariti, A., Franco, M., Denora, N., 2017. Targeting human liver cancer cells with lactobionic acid-G(4)-PAMAM-FITC sorafenib loaded dendrimers. Int. J. Pharm. 528, 485–497. https://doi.org/10.1016/j.ijpharm.2017.06.049.

Iacobazzi, R.M., Arduino, I., Di Fonte, R., Lopedota, A.A., Serratì, S., Racaniello, G., Bruno, V., Laquintana, V., Lee, B.-C., Silvestris, N., Leonetti, F., Denora, N., Porcelli, L., Azzariti, A., 2021. Microfluidic-Assisted Preparation of Targeted pH-Responsive Polymeric Micelles Improves Gemcitabine Effectiveness in PDAC. In Vitro Insights. Cancers (basel) 14, 5. https://doi.org/10.3390/cancers14010005.

Iacobazzi, R.M., Vischio, F., Arduino, I., Canepa, F., Laquintana, V., Notarnicola, M., Scavo, M.P., Bianco, G., Fanizza, E., Lopedota, A.A., Cutrignelli, A., Lopalco, A., Azzariti, A., Curri, M.L., Franco, M., Giannelli, G., Lee, B.C., Depalo, N., Denora, N., 2022. Magnetic implants in vivo guiding sorafenib liver delivery by superparamagnetic solid lipid nanoparticles. J. Colloid Interface Sci. 608, 239–254. https://doi.org/10.1016/j.jcis.2021.09.174.

Ishihara, T., Takeda, M., Sakamoto, H., Kimoto, A., Kobayashi, C., Takasaki, N., Yuki, K., Tanaka, K., Takenaga, M., Igarashi, R., Maeda, T., Yamakawa, N., Okamoto, Y., Otsuka, M., Ishida, T., Kiwada, H., Mizushima, Y., Mizushima, T., 2009. Accelerated Blood Clearance Phenomenon Upon Repeated Injection of PEG-modified PLA-nanoparticles. Pharm. Res. 26, 2270–2279. https://doi.org/10.1007/s11095-009-9943-x.

Khorshid, S., Montanari, M., Benedetti, S., Moroni, S., Aluigi, A., Canonico, B., Papa, S., Tiboni, M., Casettari, L., 2022. A microfluidic approach to fabricate sucrose decorated liposomes with increased uptake in breast cancer cells. Eur. J. Pharm. Biopharm. 178, 53–64. https://doi.org/10.1016/j.ejpb.2022.07.015.

Lam, H.T., Le-Vinh, B., Phan, T.N.Q., Bernkop-Schnürch, A., 2019. Self-emulsifying drug delivery systems and cationic surfactants: do they potentiate each other in cytotoxicity? J. Pharm. Pharmacol. 71, 156–166. https://doi.org/10.1111/jphp.13021.

Liu, Y., Wang, X., Ouyang, B., Liu, X., Du, Y., Cai, X., Guo, H., Pang, Z., Yang, W., Shen, S., 2018. Erythrocyte-platelet hybrid membranes coating polypyrrol nanoparticles for enhanced delivery and photothermal therapy. J. Mater. Chem. B 6, 7033–7041. https://doi.org/10.1039/c8tb02143k.

Mantuano, P., Boccanegra, B., Conte, E., De Bellis, M., Cirmi, S., Sanarica, F., Cappellari, O., Arduino, I., Cutrignelli, A., Lopedota, A.A., Mele, A., Denora, N., De Luca, A., 2021. β-Dystroglycan Restoration and Pathology Progression in the Dystrophic mdx Mouse: Outcome and Implication of a Clinically Oriented Study with a Novel Oral Dasatinib Formulation. Biomolecules 11, 1742. https://doi.org/10.3390/biom11111742.

Martins, J.P., Torrieri, G., Santos, H.A., 2018. The importance of microfluidics for the preparation of nanoparticles as advanced drug delivery systems. Expert Opin. Drug Deliv. 15, 469–479. https://doi.org/10.1080/17425247.2018.1446936.

Molinaro, R., Evangelopoulos, M., Hoffman, J.R., Corbo, C., Taraballi, F., Martinez, J.O., Hartman, K.A., Cosco, D., Costa, G., Romeo, I., Sherman, M., Paolino, D., Alcaro, S., Tasciotti, E., 2018. Design and Development of Biomimetic Nanovesicles Using a Microfluidic Approach. Adv. Mater. 30, 1702749. https://doi.org/10.1002/adma.201702749.

Oldenborg, P.-A., Zheleznyak, A., Fang, Y.-F., Lagenaur, C.F., Gresham, H.D., Lindberg, F.P., 2000. Role of CD47 as a Marker of Self on Red Blood Cells. Science 1979 (288), 2051–2054. https://doi.org/10.1126/science.288.5473.2051.

Othman, R., Vladisavljević, G.T., Hemaka Bandulasena, H.C., Nagy, Z.K., 2015. Production of polymeric nanoparticles by micromixing in a co-flow microfluidic glass capillary device. Chem. Eng. J. 280, 316–329. https://doi.org/10.1016/j.cej.2015.05.083.

Porcelli, L., Di Fonte, R., Pierri, C.L., Fucci, L., Saponaro, C., Armenio, A., Serratì, S., Strippoli, S., Fasano, R., Volpicella, M., Daprile, R., Tommasi, S., Ressa, C.M., Guida, M., Azzariti, A., 2022. BRAFV600E;K601Q metastatic melanoma patient-derived organoids and docking analysis to predict the response to targeted therapy. Pharmacol. Res. 182, 106323 https://doi.org/10.1016/j.phrs.2022.106323.

Racaniello, G.F., Knoll, P., Jörgensen, A.M., Arduino, I., Laquintana, V., Lopedota, A.A., Bernkop-Schnürch, A., Denora, N., 2022. Thiolation of non-ionic surfactants for the development of lipid-based mucoadhesive drug delivery systems. Eur. J. Pharm. Biopharm. 179, 95–104. https://doi.org/10.1016/j.ejpb.2022.08.015.

Rampado, R., Caliceti, P., Agostini, M., 2022. Latest Advances in Biomimetic Cell Membrane-Coated and Membrane-Derived Nanovectors for Biomedical Applications. Nanomaterials 12. https://doi.org/10.3390/nano12091543.

Rayamajhi, S., Nguyen, T.D.T., Marasini, R., Aryal, S., 2019. Macrophage-derived exosome-mimetic hybrid vesicles for tumor targeted drug delivery. Acta Biomater. 94, 482–494. https://doi.org/10.1016/j.actbio.2019.05.054.

Rennick, J.J., Johnston, A.P.R., Parton, R.G., 2021. Key principles and methods for studying the endocytosis of biological and nanoparticle therapeutics. Nat. Nanotechnol. 16, 266–276. https://doi.org/10.1038/s41565-021-00858-8.

Ricci, F., Racaniello, G.F., Lopedota, A., Laquintana, V., Arduino, I., Lopalco, A., Cutrignelli, A., Franco, M., Sigurdsson, H.H., Denora, N., 2022. Chitosan/sulfobutylether-β-cyclodextrin based nanoparticles coated with thiolated hyaluronic acid for indomethacin ophthalmic delivery. Int. J. Pharm. 622, 121905 https://doi.org/10.1016/j.ijpharm.2022.121905.

Rodriguez, P.L., Harada, T., Christian, D.A., Pantano, D.A., Tsai, R.K., Discher, D.E., 2013. Minimal "Self" Peptides That Inhibit Phagocytic Clearance and Enhance Delivery of Nanoparticles. Science 1979 (339), 971–975. https://doi.org/10.1126/science.1229568.

Serratì, S., Guida, M., Di Fonte, R., De Summa, S., Strippoli, S., Iacobazzi, R.M., Quarta, A., De Risi, I., Guida, G., Paradiso, A., Porcelli, L., Azzariti, A., 2022. Circulating extracellular vesicles expressing PD1 and PD-L1 predict response and mediate resistance to checkpoint inhibitors immunotherapy in metastatic melanoma. Mol. Cancer 21, 20. https://doi.org/10.1186/s12943-021-01490-9.

Serratì, S., Di Fonte, R., Porcelli, L., De Summa, S., De Risi, I., Fucci, L., Ruggieri, E., Marvulli, T.M., Strippoli, S., Fasano, R., Rafaschieri, T., Guida, G., Guida, M., Azzariti, A., 2023. Circulating extracellular vesicles are monitoring biomarkers of anti-PD1 response and enhancer of tumor progression and immunosuppression in metastatic melanoma. J. Exp. Clin. Cancer Res. 42, 251. https://doi.org/10.1186/s13046-023-02808-9.

Sommonte, F., Arduino, I., Racaniello, G.F., Lopalco, A., Lopedota, A.A., Denora, N., 2022. The Complexity of the Blood-Brain Barrier and the Concept of Age-Related Brain Targeting: Challenges and Potential of Novel Solid Lipid-Based Formulations. J. Pharm. Sci. 111, 577–592. https://doi.org/10.1016/j.xphs.2021.08.029.

Sommonte, F., Arduino, I., Iacobazzi, R.M., Tiboni, M., Catalano, F., Marotta, R., Di Francesco, M., Casettari, L., Decuzzi, P., Lopedota, A.A., Denora, N., 2023a. Microfluidic assembly of "Turtle-Like" shaped solid lipid nanoparticles for lysozyme delivery. Int. J. Pharm. 631, 122479 https://doi.org/10.1016/j.ijpharm.2022.122479.

Sommonte, F., Denora, N., Lamprou, D.A., 2023b. Combining 3D Printing and Microfluidic Techniques: A Powerful Synergy for Nanomedicine. Pharmaceuticals 16, 69. https://doi.org/10.3390/ph16010069.

Song, Y., Zhang, N., Li, Q., Chen, J., Wang, Q., Yang, H., Tan, H., Gao, J., Dong, Z., Pang, Z., Huang, Z., Qian, J., Ge, J., 2021. Biomimetic liposomes hybrid with platelet membranes for targeted therapy of atherosclerosis. Chem. Eng. J. 408, 127296 https://doi.org/10.1016/j.cej.2020.127296.

Stoff, R., Asher, N., Laks, S., Steinberg, Y., Schachter, J., Shapira-Frommer, R., Grynberg, S., Ben-Betzalel, G., 2023. Real world evidence of Lenvatinib + anti PD-1 as an advanced line for metastatic melanoma. Front. Oncol. 13 https://doi.org/10.3389/fonc.2023.1180988.

Sun, H., Su, J., Meng, Q., Yin, Q., Chen, L., Gu, W., Zhang, P., Zhang, Z., Yu, H., Wang, S., Li, Y., 2016. Cancer-Cell-Biomimetic Nanoparticles for Targeted Therapy of Homotypic Tumors. Adv. Mater. 28, 9581–9588. https://doi.org/10.1002/adma.201602173.

Tiboni, M., Coppari, S., Casettari, L., Guescini, M., Colomba, M., Fraternale, D., Gorassini, A., Verardo, G., Ramakrishna, S., Guidi, L., Di Giacomo, B., Mari, M., Molinaro, R., Albertini, M.C., 2021a. Prunus spinosa extract loaded in biomimetic nanoparticles evokes in vitro anti-inflammatory and wound healing activities. Nanomaterials 11, 1–14. https://doi.org/10.3390/nano11010036.

Tiboni, M., Tiboni, M., Pierro, A., Del Papa, M., Sparaventi, S., Cespi, M., Casettari, L., 2021b. Microfluidics for nanomedicines manufacturing: An affordable and low-cost 3D printing approach. Int. J. Pharm. 599, 120464 https://doi.org/10.1016/j.ijpharm.2021.120464.

Wu, Y., Wan, S., Yang, S., Hu, H., Zhang, C., Lai, J., Zhou, J., Chen, W., Tang, X., Luo, J., Zhou, X., Yu, L., Wang, L., Wu, A., Fan, Q., Wu, J., 2022. Macrophage cell membrane-based nanoparticles: a new promising biomimetic platform for targeted delivery and treatment. J Nanobiotechnology 20, 542. https://doi.org/10.1186/s12951-022-01746-6.

Yang, Q., Lai, S.K., 2015. Anti-PEG immunity: emergence, characteristics, and unaddressed questions. Wiley Interdiscip. Rev. Nanomed. Nanobiotechnol. 7, 655–677. https://doi.org/10.1002/wnan.1339.

Zanna, P., Maida, I., Grieco, C., Guida, S., Turpin Sevilla, M.C., De Summa, S., Tommasi, S., Vena, G.A., Filotico, R., Guida, G., 2013. Three novel human sporadic melanoma cell lines: signaling pathways controlled by MC1R, BRAF and β-catenins. J. Biol. Regul. Homeost. Agents 27, 131–141.

Zhang, Y., Wong, C.Y.J., Gholizadeh, H., Aluigi, A., Tiboni, M., Casettari, L., Young, P., Traini, D., Li, M., Cheng, S., Ong, H.X., 2023. Microfluidics assembly of inhalable liposomal ciprofloxacin characterised by an innovative in vitro pulmonary model. Int. J. Pharm. 635, 122667 https://doi.org/10.1016/j.ijpharm.2023.122667.

Zinger, A., 2023. Unleashing the potential of cell biomimetic nanoparticles: Strategies and challenges in their design and fabrication for therapeutic applications. J. Control. Release 358, 591–600. https://doi.org/10.1016/j.jconrel.2023.04.040.